Behavior of Iron Tetraphenylsulfonato Porphyrin Intercalated into LDH and LSH as Materials for Electrocatalytic Applications

Ali Tarhini, Juan Aguirre-Araque, Mélanie Guyot, Cyrille Costentin, Guillaume Rogez, Sylvie Chardon-Noblat, Vanessa Prevot, Christine Mousty

Behavior of iron tetraphenylsulfonato porphyrin intercalated into LDH and LSH as materials for electrocatalytic applications

Ali Tarhini[a], Juan Aguirre-Araque[b], Mélanie Guyot[c], Cyrille Costentin[c], Guillaume Rogez[b]*, Sylvie Chardon-Noblat[c]*, Vanessa Prevot[a], Christine Mousty[a]*

[a] *Université Clermont Auvergne, CNRS, Institut de Chimie de Clermont-Ferrand (ICCF), F-63000 Clermont-Ferrand, France.*
E-Mail : Christine.Mousty@uca.fr
[b] *Université de Strasbourg, CNRS, Institut de Physique et de Chimie des Matériaux de Strasbourg (IPCMS), F-67008 Strasbourg, France.*
E-mail:Guillaume.Rogez@ipcms.unistra.fr
[c] *Université Grenoble Alpes, CNRS, Département de Chimie Moléculaire (DCM), F-38000 Grenoble, France. E-mail:*
E-mail:Sylvie.Chardon@univ-grenoble-alpes.fr

Keywords: Electrocatalysis • CO_2ERR • Iron porphyrin • Layered double hydroxides • Layered simple hydroxides • Hybrid materials

Graphical abstract

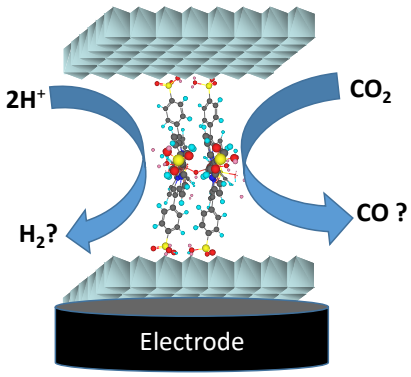

Abstract

Organic-inorganic hybrid materials were prepared by intercalation of iron 5,10,15,20 tetrakis(4-sulfonatophenyl)porphyrin complex into layered double hydroxides (ZnCr-FeTSPP LDH) and layered simple hydroxides (Zn-FeTSPP LSH) by coprecipitation. They have been characterized by ancillary techniques to compare their structural characteristics, their morphology and their ability to form films on conductive substrates in view of preparing modified electrodes for CO_2 electroreduction reaction (CO_2ERR). The electrochemical behavior of intercalated FeTSPP was studied by cyclic voltammetry (CV) showing the role of the nature and pH of aqueous electrolyte solutions on the $Fe^{III/II}$ signal. Evaluation of the CO_2ERR of ZnCr-FeTSPP modified electrode was investigated by CV and preparative scale CO_2 electrolysis in 0.1 M Na_2SO_4 aqueous solution. Whereas FeTSPP in the same electrolyte solution exhibits 18% of CO_2 conversion to CO, once intercalated into ZnCr-LDH, there is no CO formation, only H_2 (FY = 75 %). Using the ZnCr-NO_3 modified electrode, without porphyrin, the same FY of H_2 was obtained. The study illustrates the problematic and the complexity of an attractive approach for the development of innovative hybrid catalysts for heterogeneous CO_2ERR.

Introduction

Electrification of the society requires systems able to efficiently convert electricity to chemical energy and vice-versa. In that endeavour, the development of new electrolysis processes, including search of catalysts to improve selectivity and efficiency towards the desired products is essential. Among the challenges associated with setting-up new electrolysis processes, the development of modified electrodes with catalytic properties is needed. The field of modified electrodes (MEs) is vast ranging from the simple adsorption of molecular catalyst on planar electrodes to nanostructuration in tri-dimensional electrodes [1]. Immobilization of molecular catalysts for a given reaction is an attractive strategy as it offers the possibility to control active sites at the molecular level and thus, redox and catalytic properties. Moreover, incorporation of active molecular catalysts into host matrices to modify electrode surfaces gives access to the advantages of heterogeneous catalysis. On the one hand, developing supported molecular catalysis requires addressing a large number of issues such as: the choice of host material, the method of immobilization of the molecular catalyst, finding ways to transport electrons, ions and substrates within the hybrid structure. On the other hand, the strategy of heterogenization of molecular catalysts may lead to a better control of the environment of the catalytic active centre, to improve catalytic efficiency, to prevent the catalyst deactivation, to facilitate product isolation and catalyst regeneration. It gives also the possibility to perform electrolysis in aqueous electrolytes, and circumvent the limit of use of organic media where molecular catalysts are often soluble.

In the recent years, hybrid organic-inorganic materials, defined as an intimate combination at the nanoscale of organic and inorganic components, have attracted a lot of attention [2]. Some of them have been designed for sensing, separation, and catalytic conversion of CO_2 [3]. Among the inorganic host matrices, the layered structures [4], such as layered double hydroxides

(LDHs) [5] and layered simple hydroxides (LSHs) [6], constitute an attractive class of materials with advantages for immobilizing molecular catalysts in relatively accessible synthesis methods. They are of increasing interest based on their structural characteristics and their functional applications. In this family of lamellar compounds, LDHs are a versatile class described by the general formula $[M^{2+}_{1-x}M^{3+}_{x}(OH)_2]^{x+}$ $(A^{y-}_{x/y}).nH_2O$ where M^{2+} and M^{3+} are divalent and trivalent metals ions, respectively, and A^{y-} represents an y-valent anion. Regarding the LSHs, they differ from LDHs in the fact that they are composed of only divalent metal ions $M^{2+}_{2}(OH)_{4-x}A^{y-}_{x/y}.nH_2O$. One of the remarkable characteristics of these latter compounds is that the interlayer anionic species (A^{y-}) is usually coordinated to the inorganic layer metals (M^{2+}), in contrast to LDHs for which the major driving force behind intercalation of guest molecules in the interlayer spaces is related to electrostatic interactions.

Various free bases and metal porphyrins functionalized with anionic groups, i.e. sulfonates or carboxylates, were intercalated into layered hydroxide structures (LDH or LSH) having different compositions by either a conventional anion exchange of pre-formed layered materials or a direct coprecipitation procedure. For instance, the molecular catalyst FeTSPP was associated with CoAl [7], ZnCr [8] and ZnAl [9] LDH. A series of hybrid LSHs (Zn, Cu, and Co) functionalized by tetrasulfonato metal (Cu, Co)-phthalocyanines, was synthesized by an anionic exchange reaction and their electrochemical properties were investigated [10, 11]. Demel et al. have intercalated porphyrins (ZnTSPP, PdTSPP and PdTCPP (5,10,15,20-tetrakis(4-carboxyphenyl)porphyrin)) in Zn-LSH by coprecipitation to investigate the photophysical properties of these hybrids materials [12, 13]. However, to the best of our knowledge, the intercalation of FeTSPP in LSHs has never been reported so far. Some of the LDH-porphyrin hybrids have been used for their catalytic [14] or photochemical [13] properties and others to build MEs for the catalysis of electroreduction of hydrogen peroxide, dioxygen and nitrites[7, 8]. However, although inorganic materials such as LDHs and LSHs are CO_2

capture agents and potential materials for structuration at the molecular level, their use as hybrid materials for more demanding reactions, such as hydrogen evolution (HER) or CO_2 electroreduction reactions (CO_2ERR) is challenging. Indeed, the negative potential required to drive these reactions entails the risk of destabilization of the host structure or competition of the activity of the molecular catalyst with the catalytic activity of the host matrix itself.

Nonetheless, iron (III) tetraphenyl porphyrins (FeTPP) have shown high selectivity and efficient transformation of CO_2 to CO in both organic and aqueous homogeneous media following a well-known mechanism [15-19]. Heterogenization of such molecular catalyst has been done in organic-inorganic building block Metal–Organic Framework crystalline structures (Fe–porphyrin-based MOFs) [20] and carbon nanotubes (CNTs) [21] for instance, and that immobilizations have a drastic effect on CO_2 reduction catalyst efficiency and stability. Thus, inspired by such works and the catalytic properties of ZnCr-FeTSPP LDH with respect to O_2 electroreduction, we thought to investigate hybrid FeTSPP-based LDH and LSH materials as electrode modifiers for the catalysis of reductive electrolysis of saturated CO_2 aqueous solution.

In the present work, ZnCr-FeTSPP LDH and Zn-FeTSPP LSH were synthesized to compare their structural characteristics, their morphology and their ability to form films on conductive substrates in view of preparing modified electrodes for CO_2ERR. The compositions of the host layered structured based on Zn^{2+} and Cr^{3+} were selected because of their stability at low pH [8]. The electrochemical behavior of FeTSPP-based hybrid LDH was studied by cyclic voltammetry (CV) as a function of the nature and pH of aqueous electrolyte solutions under different atmospheres (Ar and CO_2). Evaluation of the CO_2ERR was finally done by preparative scale CO_2 electrolysis in aqueous solution containing sodium sulfate as electrolyte.

Experimental section

Preparation of hybrid materials

Synthesis of ZnCr-FeTSPP LDH: The hybrid LDH phase was prepared by the direct coprecipitation earlier described [8]. 0.1 M metal salt solution was prepared by dissolving 1.98 g of $Zn(NO_3)_2.6H_2O$ and 1.33 g of $Cr(NO_3)_3.9H_2O$ (R^{th} = Zn/Cr = 2) in 100 mL deionized water. 5.2 mL salt mixture (0.347 mmol Zn and 0.173 mmol of Cr) was introduced with constant flow (0.007 $mL.min^{-1}$) to a reactor containing 0.089 g (0.087 mmol) of 5,10,15,20-tetrakis-(4-sulfonatophenyl)-porphyrin-Fe(III) chloride (*Porphyrin-Laboratories GmbH, Germany*) dissolved in 8 mL deionized water under N_2 atmosphere. The amount FeTSPP was fixed as two fold-excess in charge compared to the stoichiometry. The pH was maintained constant during the coprecipitation process at a value of 6.25 by the addition of 0.2 M NaOH. After the addition, the mixture was aged for 48 h at room temperature. ZnCr-FeTSPP was recovered by centrifugation, washed twice with deionized water, and let dry in a 40°C oven overnight. It is noteworthy that FeTSPP in aqueous solution is characterized by a pH-dependent equilibrium between different monomeric and dimeric species according to the nature of axial ligands, H_2O, OH^-, O^{2-}, on the metal [22]. In the present work, we will use the notation FeTSPP as a generic name. For comparison purpose ZnCr-NO_3 phase was synthesized by coprecipitation following a similar protocol in absence of FeTSPP into the reactor. These synthetic conditions were also used to prepared Mg_2Al-LDH intercalated by FeTSPP, in this case the pH was maintained constant at a fixed value of 7.5, the pH of coprecipitation being strongly dependent on the layer metallic composition [23].

*Synthesis of Zn-FeTSPP LSH: 0.*5 g (0.458 mmol) of $(NH_4)_4$FeTSPPCl (*Porphyrin Chemicals & Engineering, France*) were dissolved in 25 mL of water and the pH was adjusted to 7.3 using a 0.2 M NaOH solution and degassed with Ar for 15 min. 0.662 g (3.497 mmol) of $Zn(NO_3)_2$ were dissolved in 15 mL of water and loaded into an addition funnel. 15 mL of H_2O containing

1.9 mmol of NaOH were loaded in another addition funnel and both solutions were added dropwise to the porphyrin solution over the course of six hours at room temperature and strong stirring (1000 rpm). The solid formed was filtered and washed thoroughly with water until the filtrate came out colorless, then washed with ethanol and dried under vacuum.

Preparation of modified electrodes

For CV analysis, modified electrodes were prepared by solvent casting on glassy carbon electrode (GCE, ϕ = 3 mm, A = 0.07 cm^2) following a procedure previously described [8, 10]. Before modification, the electrode surface was polished with 1 µm diamond paste (Presi) and washed with acetone and then it was polished again with 0.04 µm alumina slurry (Presi) to be finally rinsed with ethanol and water. Suspensions of hybrid materials (4 mg/mL) were prepared by sonication of ZnCr-FeTSPP LDH or Zn-FeTSPP LSH in water. Aliquots of 10 µL (40 µg) of these suspensions were deposited on the surface of GCE and dried under darkness for at least 2 h to ensure their complete drying before use.

Carbon paper electrodes (CPE-AvCarb MGL190 from FuelCell Store) with a larger surface area (1 cm^2/side) were used in electrolysis experiments. Hence, the geometrical surface area of all working electrodes used was 2 cm^2. They were cleaned in ultrasound bath as follow: 15 min acetone, 15 min ethanol, 15 min water and let dry in 40°C oven before the deposition of 125 µL of hybrid material suspension on both sides of the electrodes (2 x 500 µg, 500 µg cm^{-2}). The modified CPE were dried at room temperature overnight.

Considering the chemical analysis, the amounts of FeTSPP deposited on the GCE and CPE are 2.00 10^{-8} and 5.00 10^{-7} mol for ZnCr-FeTSPP|GCE and ZnCr-FeTSPP|CPE, and 1.52 10^{-8} and 3.80 10^{-7} moles for Zn-FeTSPP|GCE and Zn-FeTSPP|CPE, respectively. The stability of these films was studied using spectrometric method. The ZnCr-FeTSPP|GCE and Zn-FeTSPP|GCE modified electrodes were soaked for 1 h in 3 mL of Na_2SO_4/CO_2 (pH 4.5), then the amount of

FeTSPP released from the electrode surface into the electrolyte was determined by UV-vis spectroscopy. The molar extinction coefficient of FeTSPP (ε = 10.2 10^4 M^{-1} cm^{-1}) in aqueous acid solution (pH 4.5) was determined from the absorbance of the Soret band at 393 nm as a function of FeTSPP concentrations [24, 25]. The same procedure was performed with modified CPE, in this case the volume of electrolyte was 30 mL.

Instrumentation

Powder X-ray diffraction patterns were recorded with a Philips X'Pert automated X-ray diffractometer using CuKα radiation (λ = 0.154051 nm), over the 2–70° (2θ). FTIR spectra were recorded with a Nicolet 5,700 spectrometer from Thermo Electron Corporation using the KBr pellet technique. The metallic composition of layered materials was determined using inductively coupled plasma-atomic emission spectroscopy (ICP-AES Agilent 5800). Priori analysis, the samples were mineralized by dispersion in 6 mL of HNO_3 (69%) and 2 mL of HCl (37%) and heating at 230°C for 1 h using microwave irradiation (Anton-Paar Multiwave 5000). CHNS contents in the hybrid materials were measured using a Thermo Scientific CHNS/O FlashSmart. Intercalated FeTSPP was characterized by UV-Vis using Shimadzu *v*-2400 spectrophotometer. Thin films of ZnCr-FeTSPP and Zn-FeTSPP, prepared on ITO glass plates following the same procedure as used to prepare thin films on GCE and CPE, were analysed by transmittance under dried condition and in the presence of electrolyte solutions. The morphologies of the powders mounted on conductive carbon adhesive tabs and the films deposited on GCE or CPE were investigated with scanning electron microscopy (SEM) using a Zeiss Supra 55 FEG-VP Field-Emission Scanning Electron Microscope operating at 3 kV.

Cyclic voltammetry experiments were carried out with a BioLogic (SP-150) potentiostat using a single-compartment three-electrode cell (30 mL). Electrode potentials were reported with respect to a saturated calomel electrode reference electrode (SCE); a Pt wire was used as counter electrode. The working electrode was the ZnCr-FeTSPP│GCE. Each sample electrode was

prepared in duplicate and analysed in CV for 5 cycles to obtain a stable signal. Various electrolytes, namely $KHCO_3$, $LiClO_4$, $NaClO_4$, $KClO_4$, H_3PO_4/KH_2PO_4 buffer (PBS) and Na_2SO_4, under controlled atmospheres (Ar or CO_2) and controlled pH were used.

Controlled potential electrolyses were performed in a homemade three electrode glass electrochemical cell using a potentiostat/galvanostat ModulLab XM equipped with an external HV 100 power booster (Solartron Analytical from Ametek Scientific Instruments). Aqueous solution of 0.1 M Na_2SO_4 was used as electrolyte (volume of catholyte: 30 mL; volume of gas: 158 mL). The ZnCr-FeTSPP│CPE were used as the working electrode, only the modified surface (A = 2 cm^2) was immersed in the electrolyte. An Ag/AgCl in 3 M KCl reference electrode (Metrohm), connected to the catholyte by a Luggin capillary filled with electrolyte, was used. To convert a potential *vs.* Ag/AgCl to a potential *vs.* SCE 20 mV must be added. The counter electrode was a platinum plate connected to the solution by a frit-bridge containing the electrolyte. The aqueous electrolyte solution was bubbled at room temperature successively with Ar (20 min) and with CO_2 (20 min) until gas saturation, then the bubbling was stopped before starting electrolysis experiments under magnetic stirring (300 rpm) at different applied potentials in the cell hermetically sealed. Nevertheless, in some experiments, we observed a leakage of anolyte in the catholyte. Thus the reduction of O_2, produced by oxidation of water at the anode, could explain why the FY is not close to 100% for the electrolysis process in these particularly cases. Gaseous products were sampled from the atmosphere of the cell. CO and H_2 gases were quantitatively analysed respectively with a Perkin Elmer Clarus 500 gas chromatograph (GC) and a Perkin Elmer AutosystemXL GCs, both equipped with a 30 m molecular sieve 5 Å column and a TCD detector. For both GCs, helium was used as the carrier gas and quantification of products was insured by calibrating the gas chromatogram using a standard mixture of gases of known concentrations (5/5/5/85 v/v $H_2/CH_4/CO/sCO_2$ from Air Liquide). It should be underlined that no additional gas and liquid products to CO and H_2 were

detected by GCMS and HPLC. The faraday efficiency (FY, %) was calculated as a ratio between the number of mole of product (n^{exp}) determined by GC and the theoretical number of mole of product formed (n^{th}), calculated from the experimentally measured charge (n^{th} = Q/Fx2), knowing that the number of electrons required to form a molecule of CO or H_2 is 2 and F is the Faraday constant (96485 C mol^{-1}).

Results and Discussion

Structural and morphological characterization of hybrid compounds

Layered hybrid materials, ZnCr-FeTSPP and Zn-FeTSPP, were prepared by the direct coprecipitation method to facilitate the effective intercalation of the bulky macrocycles. The PXRD patterns of the obtained materials (Fig.1) evidenced a layered structure with a series of harmonic reflection lines corresponding to similar interlayered distances of 2.41 nm and 2.45 nm for ZnCr-FeTSPP and Zn-FeTSPP phases, respectively. All the diffraction lines can be assigned to pure layered phases with no impurities. The formation of hybrid layered hydroxide structures is confirmed by the limited number of (hkl) reflections above 30°. The interlayered values are in good agreement with the values previously reported for ZnCr-FeTSPP (2.326 nm) [8] and ZnAl-FeTSPP (2.295 nm) [9], which are consistent with the porphyrin intercalation with a perpendicular orientation of the porphyrin plane with respect to the LDH layers, the sulfonate groups interacting with adjacent positively charged sheets. Similar values have also been reported in the case of the intercalation of ZnTSPP (2.28 nm) and PdTSPP (2.22 nm) [12] within Zn-LSH, highlighting that the FeTSPP adopts a similar orientation, the nature of the metalation having no significant effect. Despite the presence of the tetrahedral Zn atoms on the hydroxide octahedral layers pointing into the interlayer domain in the case of LSH, the interlayer distances for the LSH and LDH hybrids are similar. Chemical analysis of the materials (see Supporting Information (SI)) confirmed the presence of the different elements in the materials. For the LDH a Zn/Cr ratio of 2.02 and an excess of porphyrin were evaluated,

the latter suggesting that a part of the macrocycles is adsorbed at the surface of the LDH particles. For the LSH, the analysis led to a Fe/Zn ratio of 0.078, close to the maximum theoretical loading ($Fe/Zn_{th\text{-}max} = 0.1$).

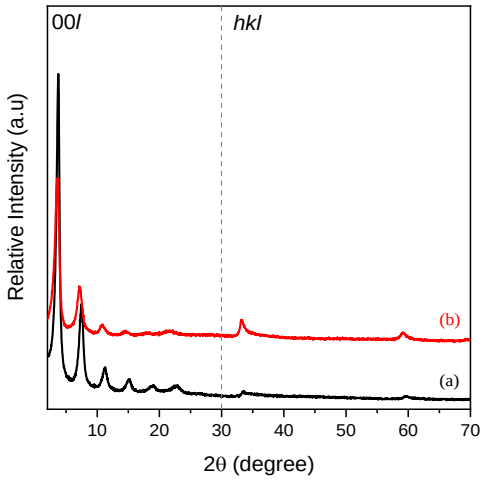

Figure 1. XRD patterns a) ZnCr-FeTSPP and b) Zn-FeTSPP

The presence of the FeTSPP within the layered structures was confirmed by FTIR (Fig.S1) and UV-Vis spectroscopies (Fig.2). The fundamental stretching vibrations ν_{as} (SO_3) and ν_s(SO_3) were observed at 1182 and 1037 cm^{-1} for ZnCr-FeTSPP and 1180 and 1037 cm^{-1} for Zn-FeTSPP, respectively. Interestingly, the position of these two bands are practically the same as that reported for the ZnAl-FeTSPP (1184 and 1039 cm^{-1}) [9] or for the non-intercalated FeTSPP (1187 and 1033 cm^{-1}), suggesting that -SO_3^- groups of intercalated porphyrins interact with the LDH or LSH layers in a similar way that is via weak interactions, *i.e.* hydrogen bonding. Previously, Demel et al. suggested that metallic TSPP were not covalently link to zinc atoms of the LSH layers [12, 13].

Aqueous solutions of FeTSPP are characterized by a pH-dependent equilibrium of monomers and dimers [22, 24, 25]. This equilibrium depends also on the medium ionic strength and on the porphyrin concentration. The UV-Vis absorption spectrum of the monomer $Fe(H_2O)_n$TSPP dissolved in acidic solution (pH 4.0) exhibits a Soret band at 394 nm and Q bands at 503 and

531 nm; whereas at pH 9.0, bands attributed to µ-oxo dimer are situated at 410 nm (Soret band), 565 and 610 nm (Q bands)[22, 25]. For comparison, a thin film of FeTSPP deposited on a quartz plate exhibits bands located at 408, 578 and 621 nm, respectively [8]. The same band positions are reported for an ultrathin film built by the layer-by-layer self-assembled technique of FeTSPP and CoAl-LDH nanosheets [7]. The red shift is consistent with strong interactions between the molecular complexes in the films. Figure 2 shows the absorption spectra of ZnCr-FeTSPP, Zn-FeTSPP and ZnCr-NO_3, prepared as thin films on ITO plates. The absorption band at 335 nm corresponds to the absorption of the LDH host matrix. For ZnCr-FeTSPP|ITO, the Soret band is centred at 422 nm and Q bands are situated at 578 and 622 nm. For Zn-FeTSPP|ITO the Soret band is situated at 414 nm. Owing to the coprecipitation pH values used in the present study, namely pH 6.25 for ZnCr-FeTSPP and 7.30 for Zn-FeTSPP, we can assume that the predominant intercalated FeTSPP species are oxo-bridged dimers $O(FeTSPP)_2$, corresponding to a Soret band red shift. This hypothesis is confirmed by the presence of a vibration band at 874 cm^{-1} on the FTIR spectrum corresponding to the Fe-O-Fe antisymmetric stretching [24] (Fig.S1).

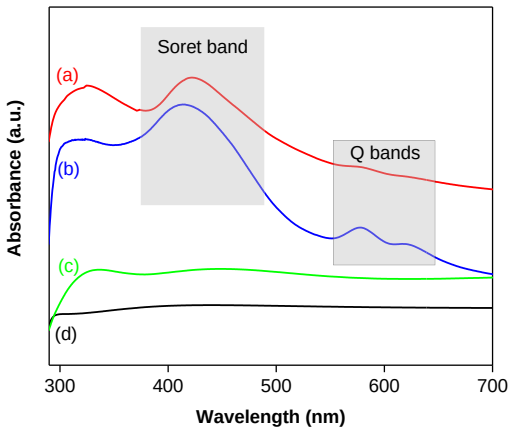

Figure 2. UV-Vis spectra of dried thin films of (a) ZnCr-FeTSPP|ITO, (b) Zn-FeTSPP|/ITO, (c) ZnCr-NO_3|ITO, (d) bare ITO.

The morphology of LDH and LSH powders (Fig. 3a and b) and the texture of the as-made thin films on glassy carbon electrode (GCE, Fig.3c and d) and on carbon paper electrode (CPE, Fig.3e and f) were analysed by SEM.

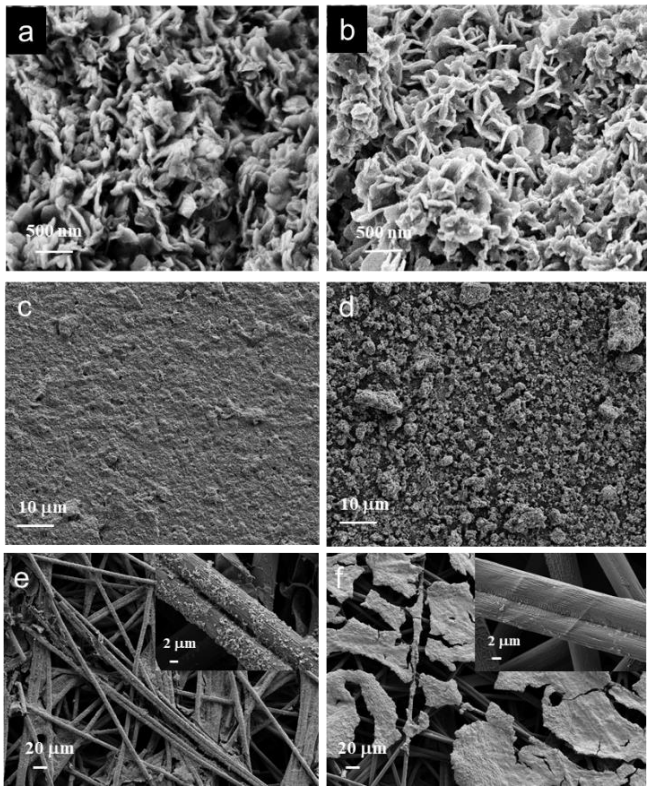

Figure 3. SEM images of hybrid powders of ZnCr-FeTSPP (a) and Zn-FeTSPP (b), and of the thin films coated on GCE (c and d) and on CPE (e and f) for ZnCr-FeTSPP and Zn-FeTSPP, respectively.

The particles of the two hybrid materials display a similar platelet like morphology with for LSH however larger platelets and a more pronounced interparticle growth. Surprisingly, the morphology of the films obtained by solvent casting differs radically whether using GCE or CPE. The ZnCr-FeTSPP dispersed in suspension led to the formation of regular and homogenous films on GCE in which the particles are well distributed (Fig.3c), while in the film obtained from Zn-FeTSPP, large particle aggregates (Fig.3d) are observed at the surface of the electrode indicating a low dispersion of the LSH platelets during the film formation. Using CPE, the LDH suspension successfully infiltrates into the carbon fibres and interacts with the surface as highlighted in the inset (Fig.3e). In the case, of Zn-FeTSPP, even if a similar protocol

was followed involving aqueous suspension, the material forms large plates at the surface (Fig.3f) and does not penetrate within the carbon paper which suggest in this case a low wettability. The carbon fibres observed at high magnification in the Zn-FeTSPP modified CPE (Fig.3e) are unmodified compared to the pristine CPE (Fig.S2).

The stability of these as-prepared films was analyzed after soaking the modified electrodes in the electrolyte (0.1 M Na_2SO_4/CO_2, pH 4.5) for 1 h. The quantification of released species was performed by an UV-Vis absorption spectrometric method. The variation of absorbance was measured at 393 nm that corresponds to the Soret band of FeTSPP in acidic solution (Fig.S3). The percentages of leaching were 17 and 12 % for ZnCr-FeTSPP|GCE or ZnCr-FeTSPP|CPE, respectively, which could be linked to a part of adsorbed FeTSPP, rather than intercalated, as evidenced by the chemical analysis (see SI). However, this percentage increased significantly for the modified electrodes prepared with Zn-FeTSPP LSH, with more than 60 % of leaching whatever the electrode used. The quality and the stability of the Zn-FeTSPP LSH thin films, prepared in the present conditions, are limited and clearly necessitate further optimization to limit the release of FeTSPP in electrolyte to be used as MEs. Therefore, Zn-FeTSPP LSH was not further studied in detail in the following and we focused only on ZnCr-FeTSPP LDH.

This study aimed at describing the potential electrocatalytic properties of FeTSPP intercalated into LDH towards CO_2ERR. The ZnCr-LDH host structure was chosen since it is reported to be stable in acid conditions [8]. The electrochemical behavior of the free FeTSPP was first investigated in aqueous solution under CO_2 atmosphere, then the electrochemical response of ZnCr-FeTSPP was investigated by CV as a thin film deposited on the surface of GCE. Evaluation of the CO_2ERR was finally done by preparative scale CO_2 electrolysis in aqueous electrolytes using modified CPE.

Electrochemical characterization of FeTSPP in aqueous electrolytes.

The electrochemical behavior of water soluble FeTSPP is known to be pH dependent according to the nature of axial ligands (H_2O, OH^-, O^{2-}) on the metal centre [26-28]. In acidic media the FeTSPP monomer is favored but a µ-oxo-bridged dimer is detected in basic solutions [22, 24, 25]. This latter species shows a slow heterogeneous charge transfer without any well-defined electrochemical signal in CV [26]. As shown in figure 4, in 0.1 M $KHCO_3$ at pH 8.6 (curve a and inset), an irreversible wave is observed at -1.2 V *vs.* SCE which may correspond to the irreversible reduction of $Fe^{II/I}$ [26]. A well-defined $Fe^{III/II}$ signal is not observable in these pH conditions in line with a chemically slow µ-oxo-dimer dissociation prior to reduction thus leading to a chemically limited CE mechanism [29]. The $Fe^{I/0}$ redox process is also hardly discernible since it is concomitant to the hydrogen evolution reaction (HER). However, this third wave is the wave of interest for CO_2 electrocatalytic activation [30]. In the presence of CO_2, the pH of the electrolyte solution (H_2O + 0.1 M $KHCO_3$) decreases to 6.4 and the features of the successive reduction of the initial µ-oxo dimer are modified. An increase of the catalytic cathodic current at -1.60 V is observed (Fig.4, curve b). However, the catalytic wave shows a crossing of the forward and backward CV traces, indicating an increase of the catalytic current as time is passing by. This behavior is often due to an evolution of the initial catalyst toward a more efficient catalytic species that might be deposited on the electrode surface [31]. In 0.1 M Na_2SO_4 upon CO_2 saturation atmosphere (pH 4.5), the well-defined reversible redox couple $Fe^{III/II}$ of the monomeric form of FeTSPP is recovered at $E_{1/2}$ = -0.28 V and an intense cathodic peak appears at -1.49 V which may probably be due to the catalytic reduction of CO_2 (Fig. 4, curve c). We again note a trace crossing in the CV presumably indicating an evolution of the iron porphyrin catalyst at highly negative potentials. In order to verify the ability of the electrogenerated Fe^0TSPP to catalyse the CO_2ERR, a controlled potential electrolysis was performed in an aqueous solution of 0.45 mM FeTSPP in 0.1 M Na_2SO_4 under CO_2 atmosphere

at an applied potential -1.45 V (negative enough to observe catalysis but positive enough to prevent catalyst evolution). After the passage of Q = 22 C, analysis of the headspace gas led to a faradaic yield (FY) of 18 % of CO_2-to-CO conversion and 60 % of hydrogen production. Replacing the Na_2SO_4 electrolyte by a phosphate buffer (PBS, pH 4.5, E^{app} -1.60 V) leads to the exclusive formation of H_2. This is in line with previously reported results for CO_2ERR with a water soluble iron porphyrin catalyst showing that addition of phosphate buffer promotes the catalytic HER over the competing CO_2-to-CO conversion [30]. These CO_2 electrolysis results, obtained with homogeneous FeTSPP aqueous solutions, show that this molecular catalyst can be used for the conversion of CO_2, but with some limitations regarding its selectivity, the nature of electrolyte and hence the catalyst environment. In the context of the present work, the questions are: (i) what is the catalytic behavior of FeTSPP when it is intercalated in the LDH material and (ii) what is the role of the ZnCr-LDH matrix in the hybrid catalyst material on the electrochemical reaction?

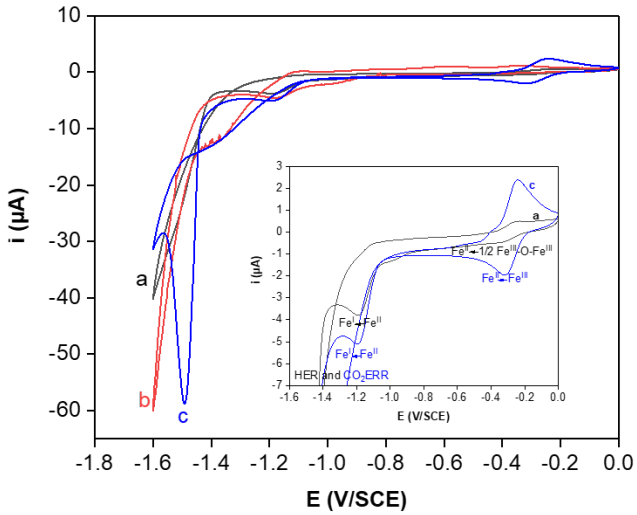

Figure 4. Cyclic voltammograms of 0.5 mM FeTSPP (GCE, v = 50 mV s^{-1}) in different aqueous electrolytes a) 0.1 M $KHCO_3$ under Ar at pH 8.6 (black curve), b) 0.1 M $KHCO_3$ under CO_2 at pH 6.8 (red curve) and c) 0.1 M Na_2SO_4 under CO_2 at pH 4.5 (blue curve). Inset shows a zoom of a and c curves between -1.60 and 0 V.

Electrochemical characterization of Fe^{III} in ZnCr-FeTSPP

To assess the electroactivity of the metallic centres in ZnCr-FeTSPP, CV measurements were conducted in different aqueous electrolytes ($LiClO_4$, $NaClO_4$, $KClO_4$, and Na_2SO_4, 0.1 M in H_2O) in a potential range between 0 and -0.50 V *vs.* SCE. From XDR, UV-Vis and FTIR data, we can assume that µ-oxo dimers are present within the interlayer space of ZnCr-LDH host matrix [8]. We studied the evolution of UV-Vis spectra of ZnCr-FeTSPP|ITO thin films dried and when they were soaked in aqueous electrolyte solutions saturated under Ar or CO_2 and/or as a function of pH (Fig.S4). The UV-Vis spectra were recorded directly in the cuvette. When the ZnCr-FeTSPP film is hydrated, a shift of the Soret band towards the lower wavelength is observed. In $LiClO_4$ under Ar or CO_2 (pH fixed at 4.5) or in Na_2SO_4/Ar (pH 8.6) it is located at 412 nm. This band shifts to 394 nm with a shoulder at 412 nm in the latter electrolyte saturated with CO_2, which induces the pH decrease to pH 4.5. This illustrates the evolution of the species present in the film as a function of the pH of the medium. The position of the Soret bands depending on the conditions are summarized in Table S1.

As observed for the FeTSPP in aqueous solution, this immobilized µ-oxo-dimer species gives an ill-defined electrochemical signal in neutral pH in line with a reduction of the Fe^{III} centres preceded by a chemically slow µ-oxo-dimer dissociation [8]. Since the monomer is favored in acidic medium, the pH of the electrolyte solutions was fixed at 4.5. In 0.1 M $LiClO_4$ under Ar, a small reduction signal is observed around -0.30 V (Fig. 5A, curve a). In the presence of CO_2, an increase of the signal reversibility was systematically observed whatever the electrolyte used (*i.e.* in $LiClO_4$ Fig.5A curve b). The presence of carbonate might favor the monomer species over the µ-oxo-dimer. Moreover, the peak intensity depends on the cation ($Li^+ < Na^+ < K^+$) and also the anion (ClO_4^- or SO_4^{2-}) of the electrolyte (Fig. 5B). The best response was obtained in Na_2SO_4 under CO_2 with a one-electron $Fe^{III/II}$ reversible signal at $E_{1/2}$ = -0.27 V *vs.* SCE with a ΔEp = 55 mV, close to the observed potential value of the of $Fe^{III/II}$ redox system of the FeTSPP

in solution ($E_{1/2}$ = -0.28 V), measured in the same electrolyte condition (see above). It should be noted that the current intensity of this $Fe^{III/II}$ signal is particularly small compared to the electrochemical signals previously reported for other electroactive anions intercalated in LDH, such as anthraquinone sulfonates [32], ferrocene sulfonates [33] or 2,2'-azino-bis(3-ethylbenzthiazoline-6-sulfonate [34]. Due to a charge balancing effect, the amount of intercalated FeTSPP, bearing four sulfonate groups, is at least two or four times lower than disulfonate or monosulfonate anions. Moreover, this iron complex must be in a specific coordination to be electroactive.

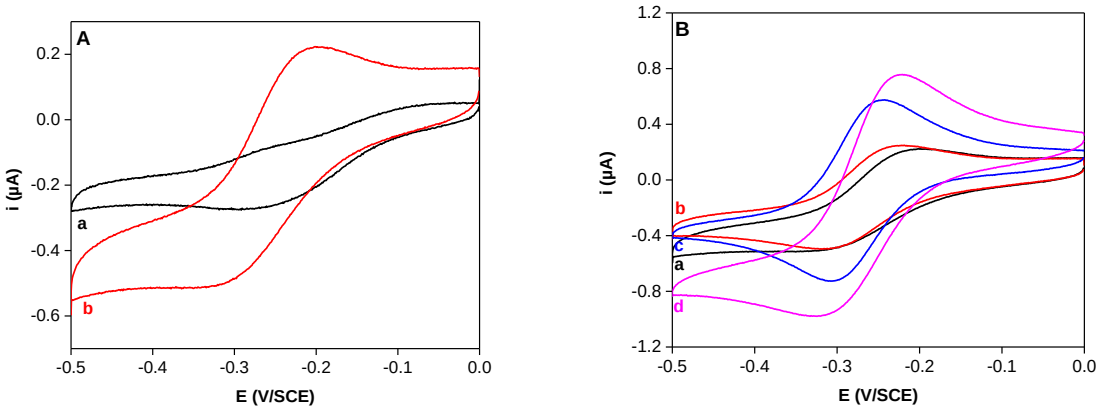

Figure 5. Cyclic voltammograms of ZnCr-FeTSPP|GCE (5th cycle) **A)** in 0.1 M $LiClO_4$ a) under Ar, b) under CO_2; **B)** under CO_2 in a) 0.1 M $LiClO_4$, b) $NaClO_4$, c) $KClO_4$, d) Na_2SO_4 (pH 4.5, v = 50 mV s^{-1}).

In Na_2SO_4 electrolyte under CO_2, the peak intensities (Ip_a and Ip_c) varied as a function of $v^{1/2}$ in the 10-100 mV s^{-1} range (Fig.6), indicating that the reduction process of immobilized FeTSPP, inside the LDH, is under diffusion control. Knowing the amount of FeTSPP immobilized on the electrode surface (2 10^{-8} moles) and the thickness of the film (~ 2 µm) estimated from SEM image, an apparent diffusion coefficient (D^{app}) in the range of 10^{-14} cm^2 s^{-1} is obtained. The observed effect of the electrolyte composition is indicative that the diffusive behavior of the charge transport within the film is certainly limited by ion displacement for charge compensation within the film. This very low value for D^{app} appears to be in line with the

observation of regular and dense homogenous films on GCE (Fig.3c). It is certainly a limitation for the catalytic application since only a small amount of immobilized FeTSPP is expected to be electrocatalytically active as only a thin diffusion-reaction layer will develop, which size is $\sqrt{\frac{Dapp}{kcat}}$ (k_{cat} is the apparent catalytic rate in s^{-1}) and therefore proportional to the square root of D^{app}. Nonetheless, the aspect of LDH on CPE (Fig.3e) showing a less dense deposit seems to indicate that the expected limitation might be much less severe on CPE (used as catalyst support for electrolysis) than on GCE (used for CV).

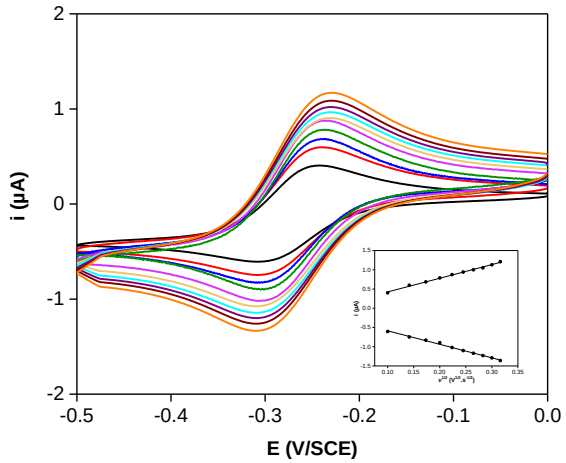

Figure 6. Cyclic voltammograms of ZnCr-FeTSPP|GCE in 0.1 M Na_2SO_4 under CO_2 at pH 4.5 ($10 \leq v \leq 100$ mV s^{-1}). Insert shows the evolution of Ip_a and Ip_c as function of $v^{1/2}$.

Electrocatalytic response in the presence of CO_2

As shown in figure 4 for the FeTSPP in aqueous solution, the CO_2 electrocatalysis process occurs at a cathodic potential corresponding to the reduction of Fe^I. Therefore, the electrochemical response of ZnCr-FeTSPP was studied in 0.1 M Na_2SO_4 over a wider potential range (Fig.7). A significant increase of the electrochemical signal is observed in the presence of CO_2 (curve b) compared to the signal obtained under Ar (curve a). However, the new peak observed at -1.50 V is associated on the reverse scan with an irreversible anodic wave at -1.00 V. This irreversible redox system was observed in all investigated electrolytes. Comparing the

CV of ZnCr-FeTSPP with a reference LDH containing no porphyrin (ZnCr-NO_3, Inset Fig.7), one can assume that these peaks can be associated with the presence of Zn^{2+} in the LDH matrix [35-37]. It should be noted that the position and intensity of the anodic peak depend strongly on the presence of CO_2, and then on the pH of the solution.

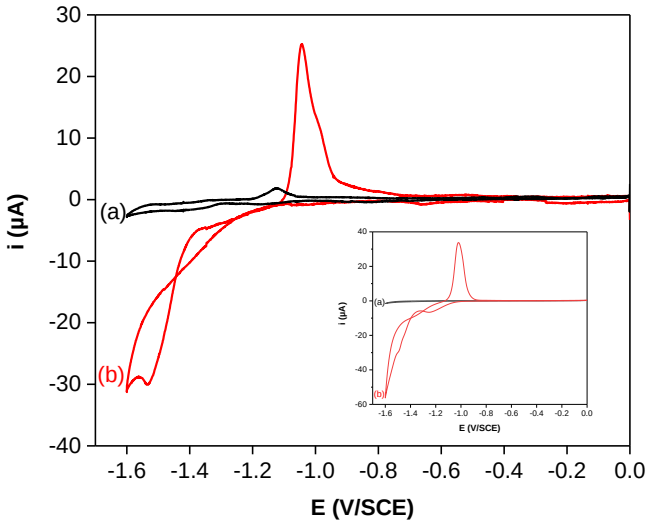

Figure 7. Cyclic voltammograms of ZnCr-FeTSPP | GCE, in 0.1 M Na_2SO_4 under a) Ar pH 8.6, b) CO_2 pH 4.5 (5^{th} cycle, v = 50 mV s^{-1}). Inset: ZnCr-NO_3 | GCE in the same condition

Considering these data, electrolyses were conducted in 0.1 M Na_2SO_4 using CPE modified electrodes with a larger geometrical surface (2 cm^2) at -1.40 and -1.50 V, in agreement with what was performed for porphyrin in solution. Unfortunately, at these applied potentials the catalytic currents were too low and do not provide an efficient catalytic process. At a more cathodic potential (E^{app} = -1.60 V) with a ZnCr-FeTSPP | CPE electrode, there is no CO formation and only H_2 is detected (FY = 75%; Table 1). Using a LDH containing no Fe-porphyrin (ZnCr-NO_3), we obtain the same faradaic yield of H_2, with low efficiency (Table 1), in line with the CVs shown in figure 7 indicating that at -1.6 V the current is dominated by the redox activity of the LDH matrix. These results show that the catalytic electrochemical process takes place mainly on the ZnCr-based LDH part of the hybrid material. Indeed, the very slow

apparent diffusion coefficient (D^{app}) of the charge transport required for activation of FeTSPP would only make a very tiny amount of CO_2ERR catalyst available.

Table 1. Electrolysis data obtained with LDH|CPE modified electrodes in 0.1 M Na_2SO_4 under CO_2 atmosphere (pH 4.5), E^{app} =-1.60 V.

LDH	**ZnCr-FeTSPP**	**ZnCr-NO_3**	**MgAl-FeTSPP**
Current (mA)	6.2	2	3
FY CO (%)	<1	<1	3
FY H_2 (%)	<75	<73	97

In order to prevent the role of Zn that we thought was harmful in the LDH hybrid material for catalysis of the CO_2ERR (see above), MgAl-FeTSPP was prepared and its electrochemical behavior was studied in Na_2SO_4 (Fig.8). In this case, the MgAl-based LDH matrix appears electrochemically inactive but it is likely to be more unstable under CO_2 due to the acidic pH conditions [23]. With MgAl-FeTSPP|GCE under Ar (curve a), two reversible redox couples appear at $E_{1/2}$ = -0.46 and -1.14V *vs.* SCE that could correspond to the $Fe^{III/II}$ and $Fe^{II/I}$ redox systems. However contrary to what has been observed for FeTSPP in ZnCr-LDH, these peaks appear even under a basic condition (pH 8.6) and their potentials are shifted towards more cathodic values. This suggests that the Fe-porphyrin environment is different in both types of hybrid LDH materials, as confirmed with the position of the Soret band (Fig. S5 and Table S1). FeTSPP is more favorable to aggregate when it is intercalated in ZnCr-LDH (Fig.S4) than in Mg_2Al-LDH host structure. These results may be related to the highly ordered ZnCr hydroxide layer leading to structural constraint accompanying FeTSPP intercalation [8, 38]. Under CO_2 saturated atmosphere (Fig.8, curve b), these two reversible peaks disappear to give way to two reduction waves that start at -1.30 V and -1.40 V/SCE. The cathodic currents are in the same range than those observed with ZnCr-LDH and significantly higher than that obtained with Mg_2Al-NO_3|GCE (Fig.8, curve c). During the return scan, an anodic peak appears at a potential of -0.32 V.

In order to know the activity of this new Zn free hybrid material deposited on CPE, an electrolysis was conducted in the same experimental conditions than with ZnCr-FeTSPP at -1.60 V (Table 1). With a MgAl-FeTSPP|CPE electrode the major product detected is also H_2 (FY = 97%), confirming the poor catalytic behavior for CO_2ERR of immobilized FeTSPP when it is intercalated in the LDH materials, and also the non-innocent role of the LDH matrices and/or FeTSPP towards HER, the competitive CO_2ERR reaction in aqueous electrolytes.

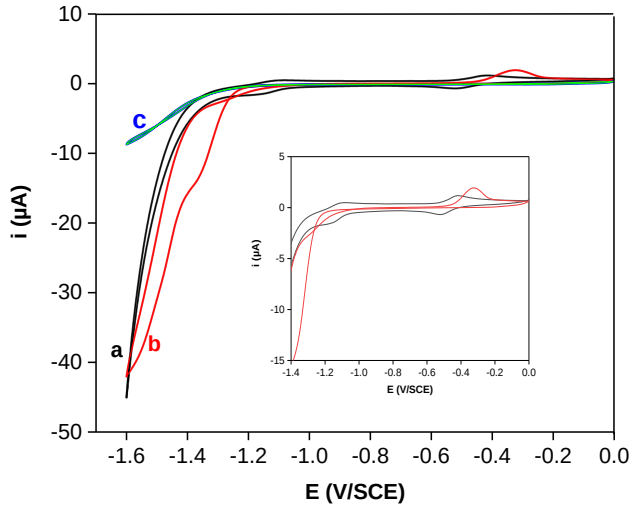

Figure 8. Cyclic voltammograms of MgAl-FeTSPP|GCE in 0.1 M Na_2SO_4 under a) Ar pH 8.6, b) CO_2 pH 4.5 and c) MgAl-NO_3|GCE in 0.1 M Na_2SO_4 under CO_2 (v = 50 mV s^{-1}). Inset shows a zoom of a and b curves between -1.40 and 0 V.

Conclusion

An anionic iron-porphyrin (FeTSPP) was intercalated between ZnCr-LDH and Zn-LSH layers using a coprecipitation method at constant pH. Structural and UV-Vis spectrometric characterizations show the intercalation of the guest molecule as an oxo-bridged diron(III) complex with a perpendicular arrangement of the porphyrin ring with respect to the hydroxide layers. While a small contribution of monomers (<1%) can be taken into account in the electrochemical responses of ZnCr-FeTSPP at pH 4.5 (0.1 M Na_2SO_4), the electrocatalytic properties of this hybrid material for CO_2 electroreduction reaction was investigated for the first time, showing that the major product detected was H_2 which results from the competitive HER.

This study of hybrid catalytic materials illustrates the problematic and the complexity of an attractive approach for the development of innovative solid hybrid catalysts based on LDH and LSH for CO_2ERR which is challenging due to the negative potential required to drive this reaction. It reveals the main drawbacks of the iron porphyrin immobilization in various LDH on its catalytic activity towards CO_2ERR. In conclusion, it appears essential to immobilise molecular catalysts that are very efficient for CO_2ERR, to choose a host matrix with an open structure that is favourable to the diffusion of ions and electrons and does not have competitive catalytic properties such as HER. This is the challenge we will face and we want to address by continuing this project, by developing other materials in that direction.

Supplementary Information The online version contains supplementary material available at….

Declarations

Ethical Approval and Consent to participate not applicable

Human Ethics not applicable

Consent for publication not applicable

Availability of supporting data: All data generated or analyzed during this study are included in this article and in the supplementary material.

Competing interests The authors declare no competing interests

Funding This work was supported by the French National Research Agency ($CALHYCO_2$ - ANR-19-C05-0015)

Author's Contributions All authors contributed equally to the study conception, design and data analysis. Material preparation and data collection were performed by Ali Tarhini, Juan Aguirre-Araque and Mélanie Guyot. The first draft of the manuscript was written by Christine Mousty and all authors commented on previous versions of the manuscript. All authors read and approved the final manuscript submitted to this journal.

Acknowledgements The authors would like to thank the French ANR ($CALHYCO_2$ - ANR-19-C05-0015) for their financial support, in particular AT, MG and JA-A for their doctoral fellowship or post-doctoral grant. We would like to thank also Pr. Claude Forano (ICCF) for his help in chemical analysis and Florian Molton (DCM) for his technical assistance. Technical

platforms of ICCF and IPCMS are acknowledged for access to the SEM and X-Ray diffractometers.

Authors' information Juan Aguirre-Araque (ORCID 0000-0002-3442-5248); Cyrille Costentin (ORCID 0000-0002-7098-3132); Guillaume Rogez (ORCID 0000-0001-9006-7273); Sylvie Chardon-Noblat (ORCID 0000-0003-0273-1571); Vanessa Prevot (ORCID 0000-0001-6250-7550); Christine Mousty (ORCID 000-0002-3003-2092).

References

[1] C. Costentin, J.-M. Savéant, Curr. Opin. Electrochem. 15, 58 (2019).

[2] L. Nicole, C. Laberty-Robert, L. Rozes, C. Sanchez, Nanoscale 6, 6267 (2014).

[3] M. Rebber, C. Willa, D. Koziej, Nanoscale Horizons 5, 431 (2020).

[4] F.M. Fernandes, H. Baradari, C. Sanchez, Appl. Clay Sci. 100, 2 (2014).

[5] C. Taviot-Guého, V. Prévot, C. Forano, G. Renaudin, C. Mousty, F. Leroux, Adv. Funct. Mater. 28, 1703868 (2018).

[6] G. Rogez, C. Massobrio, P. Rabu, M. Drillon, Chem. Soc. Rev. 40, 1031 (2011).

[7] M.F. Shao, J.B. Han, W.Y. Shi, M. Wei, X. Duan, Electrochem. Commun. 12, 1077 (2010).

[8] C. Taviot-Gueho, M. Halma, K. Charradi, C. Forano, C. Mousty, New J. Chem. 35, 1898 (2011).

[9] M. Halma, K. Aparecida Dias de Freitas Castro, C. Taviot-Gueho, V. Prévot, C. Forano, F. Wypych, S. Nakagaki, J. Catal. 257, 233 (2008).

[10] S. Eyele-Mezui, P. Vialat, C. Higy, R. Bourzami, C. Leuvrey, N. Parizel, P. Turek, P. Rabu, G. Rogez, C. Mousty, J. Phys. Chem. C 119, 13335 (2015).

[11] R. Bourzami, S. Eyele-Mezui, E. Delahaye, M. Drillon, P. Rabu, N. Parizel, S. Choua, P. Turek, G. Rogez, Inorg. Chem. 53, 1184 (2014).

[12] J. Demel, P. Kubat, I. Jirka, P. Kovar, M. Pospisil, K. Lang, J. Phys. Chem. C 114, 16321 (2010).

[13] J. Demel, K. Lang, Eur. J. Inorg. Chem. 2012, 5154 (2012).

[14] S. Nakagaki, K.M. Mantovani, G. Sippel Machado, K.A. Dias de Freitas Castro, F. Wypych, Molecules 21, 291 (2016).

[15] K. Torbensen, C. Han, B. Boudy, N. von Wolff, C. Bertail, W. Braun, M. Robert, Chem. Eur. J. 26, 3034 (2020).

[16] G.F. Manbeck, E. Fujita, J. Porphyr. Phthalocyanines 19, 45 (2015).

[17] J. Wu, Y. Huang, W. Ye, Y. Li, Adv. Sci. 4, 1700194 (2017).

[18] E. Boutin, L. Merakeb, B. Ma, B. Boudy, M. Wang, J. Bonin, E. Anxolabéhère-Mallart, M. Robert, Chem. Soc. Rev. 49, 5772 (2020).

[19] C. Costentin, M. Robert, J.-M. Savéant, Chem. Soc. Rev. 42, 2423 (2013).

[20] B.-X. Dong, S.-L. Qian, F.-Y. Bu, Y.-C. Wu, L.-G. Feng, Y.-L. Teng, W.-L. Liu, Z.-W. Li, ACS Appl. Energy Mater. 1, 4662 (2018).

[21] M. Abdinejad, A. Seifitokaldani, C. Dao, E.H. Sargent, X.-a. Zhang, H.B. Kraatz, ACS Appl. Energy Mater. 2, 1330 (2019).

[22] P. Böhm, H. Gröger, ChemCatChem 7, 22 (2015).

[23] C. Forano, U. Costantino, V. Prevot, C. Taviot-Gueho, Chapter 14.1 - Layered Double Hydroxides (LDH), in: F. Bergaya, G. Lagaly (Eds.) Developments in Clay Science, Elsevier, 2013, pp. 745.

[24] E.B. Fleischer, J.M. Palmer, T.S. Srivastava, A. Chatterjee, J. Am. Chem. Soc. 93, 3162 (1971).

[25] S.C.M. Gandini, V.E. Yushmanov, M. Tabak, J. Inorg. Biochem. 85, 236 (2001).

[26] M.H. Barley, T.J.J.J.o.t.A.C.S. Meyer, J. Am. Chem. Soc. 108, 5876 (1986).

[27] S.-M. Chen, J. Electroanal. Chem. 407, 123 (1996).

[28] S.-M. Chen, Electrochim. Acta 42, 1663 (1997).

[29] J.-M. Savéant, C. Costentin, in: Elements of Molecular and Biomolecular Electrochemistry: An Electrochemical Approach to Electron Transfer Chemistry, John Wiley & Sons,, 2019, pp. 97.

[30] C. Costentin, M. Robert, J.-M. Savéant, A. Tatin, PNAS 112, 6882 (2015).

[31] K.J. Lee, B.D. McCarthy, J.L. Dempsey, Chem. Soc. Rev. 48, 2927 (2019).

[32] C. Mousty, S. Therias, C. Forano, J.-P. Besse, J. Electroanal. Chem. 374, 63 (1994).

[33] C. Mousty, C. Forano, S. Fleutot, J.C. Dupin, Electroanalysis 21, 399 (2009).

[34] S. Therias, C. Mousty, C. Forano, J.P. Besse, Langmuir 12, 4914 (1996).

[35] X. Fan, Z. Yang, X. Xie, W. Long, R. Wang, Z. Hou, J. Power Sources 241, 404 (2013).

[36] R. Wang, Z. Yang, B. Yang, T. Wang, Z. Chu, J. Power Sources 251, 344 (2014).

[37] J. Huang, Z. Yang, T. Wang, Electrochim. Acta 123, 278 (2014).

[38] C. Taviot-Guého, Y. Feng, A. Faour, F. Leroux, Dalton Trans. 39, 5994 (2010).